

Kohn-Luttinger effect in nested Fermion liquids

Hyok-Jon Kwon*

Department of Physics, Brown University, Providence, RI 02912-1843, USA

(October 2, 1996)

cond-mat/9610020

We study the Kohn-Luttinger effect in a two-dimensional nested Fermion liquid with a repulsive interaction via the renormalization group (RG) method and identify the resulting order parameter symmetry. Using the band structure of the 2D Hubbard model close to half-filling as a prototype, we construct the effective low-energy theory. We use multidimensional bosonization to incorporate the zero sound channel and find marginal Fermi liquid behavior in the absence of any instability. We show an analog of the Landau theorem in nested Fermion liquids, which serves as the criterion of the BCS instability. Including repulsive or antiferromagnetic exchange interactions in the low-energy theory, we show that the $d_{x^2-y^2}$ -wave BCS channel is renormalized to be the most attractive. Below half-filling, when the nesting is not perfect, there is competition between the spin-density-wave (SDW) and the BCS channels; when the SDW coupling is small enough, there occurs a $d_{x^2-y^2}$ -wave superconducting instability at sufficiently low temperatures.

PACS numbers: 11.10.Hi, 71.10.Hf, 74.20.Mn, 74.25.-q

I. INTRODUCTION

One question of recent interest concerns the possible breakdown of the Fermi liquid in the presence of singular or even regular interactions. One example is the Luttinger liquid in one spatial dimension where the quasiparticle pole is destroyed by a short-range interaction although in this case the low-energy excitation remains gapless. The existence of the Luttinger liquid in higher spatial dimensions has also been proposed but is still controversial.¹ Another example is the Kohn-Luttinger (KL) effect: a Fermi liquid state is unstable against one or more BCS channels in the presence of a repulsive interaction.² It has been shown that a short-range repulsive interaction can induce an attractive BCS channel at large orbital angular momentum modes. In three-dimensional Fermi gas, the Kohn-Luttinger effect was found in the p -wave BCS channel.³ This notion was extended to two-dimensional Fermi liquids and a weaker KL effect was also found in the p -wave channel although the effect is not visible in a second order perturbative expansion.⁴

However, the KL effects in isotropic Fermi liquids are weak because they are found in sub-leading corrections in the renormalization group (RG) sense; the resulting T_c is expected to be low. For example, in three dimensions, the KL correction to the beta function is found to be $O(s^{-7/4})$ where s is the dimensionless length scale which is taken to be a large number in the low-energy limit.¹¹ But in the case of nested Fermion liquids, the effect is more dramatic since the nesting gives rise to a logarithmic flow in the repulsive channel. Baranov et al.³ studied the KL effect in a two-dimensional Hubbard model at low filling factors where the Fermi surface is almost circular and found an attractive channel with d_{xy} -wave symmetry, but it is also a sub-leading effect which originates from the directional property of the square lattice. In this paper we study the KL effect in two dimensions in a nested square Fermi surface.

The subject of this paper may be of interest in the context of the cuprate high T_c superconducting materials. The KL effect implies that an initially repulsive interaction between electrons can induce an effective attractive BCS interaction among quasiparticles lying in the thin momentum shell around the Fermi surface. Hence this is one possible candidate for a non-phononic mechanism for cuprate superconductivity. Indeed, we find that the repulsive interaction, which naturally contains an antiferromagnetic (AF) exchange channel, favors a $d_{x^2-y^2}$ -wave BCS instability. This is in accord with expectations.⁵

The low-energy theory of the two-dimensional Hubbard model is complicated by several features of the anisotropic Fermi surface. Especially near half-filling, there are van Hove singularities in addition to non-uniformity of the Fermi velocities along the Fermi surface. Moreover, in the low-energy limit, the system is not a regular Fermi liquid due to nesting. For instance, the quasiparticles are expected to have a short lifetime, $1/\tau \sim T$ near the Fermi surface, and the existence of a well-defined Fermi surface may be questioned.⁶ To incorporate these characteristics, we introduce a low-energy theory which models the band structure of the two-dimensional Hubbard model near half-filling. We make use of multidimensional bosonization⁷⁻¹⁰ to describe the low-energy properties of the model. Although Fermi liquid theory may break down near the Fermi surface, marginal deviations from a Fermi liquid are within the scope of bosonization.

The RG in the bosonic basis is a suitable method to study the low-energy phases of the model since it puts all interaction channels on an equal footing. Wilson's RG algorithm, which we shall make use of, consists of integrating out high-energy degrees of freedom to construct a low-energy effective theory. In a degenerate fermion system, this amounts to successively eliminating inner and outer sides of the momentum shell around the Fermi surface in which the low-energy theory lies.^{11–13} In this paper we construct a low-energy effective theory of a nested fermion liquid by the RG procedure and then investigate the RG flow of the effective interactions in the framework of bosonization. In other words, we successively integrate out higher energy modes of the bosonic field ϕ . In most cases, this bosonized RG procedure yields results which agree with those obtained in the fermion basis. The distinct advantage of the RG treatment based on bosonization is that the existence of well-defined quasiparticles is not a priori assumed. Furthermore, those interaction channels which preserve the infinite- $U(1)$ symmetry⁷ on the Fermi surface are exactly diagonalized at the outset.¹⁴

This paper is organized as follows. In Sec. II, we introduce the model low-energy theory of a two-dimensional nested Fermion liquid. We use multidimensional bosonization to incorporate the zero sound channel and show that the resulting low-energy fixed point is a marginal Fermi liquid. In Sec. III, we derive the RG equations for the BCS channel and discuss the condition of the BCS instability. An analog of Landau theorem is applicable to the case of anisotropic Fermi surface. In Sec. IV, we incorporate marginally relevant repulsive or AF interactions and evaluate their RG flow which contribute to the BCS channel. The $d_{x^2-y^2}$ -wave channel is the most important one, and we argue that below half-filling competition arises between the SDW and $d_{x^2-y^2}$ -wave superconductivity. A brief summary and conclusions are given in Sec. V.

II. MODEL LOW-ENERGY THEORY

The Hubbard model is a convenient description of strongly correlated fermion systems. For a reliable investigation into the RG of this model, it is essential to accommodate properly realistic band structure near the Fermi surface. Here we present a model low-energy theory which simulates the nested fermion system.

First, consider the band structure of Hubbard model in two dimensions near half-filling. The Hamiltonian is:

$$H = -t \sum_{i,j} c_i^{\dagger\alpha} c_{j\alpha} + U \sum_i n_{i\uparrow} n_{i\downarrow} \quad (1)$$

where i, j are between nearest neighbors on a square lattice and U is the on-site interaction strength. Here $c_i^{\dagger\alpha}$ and $c_{i\alpha}$ are fermion creation and annihilation operators. Throughout this paper we assume that $|U/t| \ll 1$ holds so that the perturbative expansions are justified. For now we turn off the on-site interaction term and discuss the character of the Fermi surface that results from the hopping term. The spectrum of the fermions is

$$E(\mathbf{k}) = -2t(\cos k_x a + \cos k_y a), \quad (2)$$

where a is the lattice spacing. At half-filling, the Fermi surface is described by the points in k -space which satisfy

$$\cos k_x a + \cos k_y a = 0. \quad (3)$$

The Fermi velocity is a function of \mathbf{k} given by

$$\mathbf{v}(\mathbf{k}) = 2ta(\hat{\mathbf{x}} \sin(k_x a) + \hat{\mathbf{y}} \sin(k_y a)) \quad (4)$$

on the Fermi surface. Singularities in the density of states occur at four corners of the Fermi surface, $\mathbf{k} = (\pm\pi/a, 0)$ or $(0, \pm\pi/a)$, where the Fermi velocity vanishes.

Turning on the on-site interaction, the RG may be used to integrate out the high-energy degrees of freedom.¹¹ The resulting low-energy effective theory is expressed in terms of quasiparticles living in a narrow shell around the Fermi surface of energy cutoff ε_c . Quasiparticles may then be related to the bare fermion operators by

$$\psi_{\mathbf{k}} = Z_{\mathbf{k}}^{-1/2}(\varepsilon_c) c_{\mathbf{k}}, \quad (5)$$

where the wave-function renormalization factor $Z_{\mathbf{k}}(\varepsilon_c)$ rescales the discontinuity in the quasiparticle occupancy at the Fermi surface back to one. The final quasiparticle weight $Z_{\mathbf{k}}$ can be obtained by further integrating out the remaining low-energy degrees of freedom, $\lim_{\varepsilon_c \rightarrow 0} Z_{\mathbf{k}}(\varepsilon_c) = Z_{\mathbf{k}}$. In non-Fermi liquids, $Z_{\mathbf{k}}$ is zero. Here we stop the RG process at the energy scale ε_c and investigate the low-energy theory thus obtained. Assuming that the weak nearest-neighbor

interaction term does not alter the shape of the Fermi surface or the band structure in Eq. (2), we may linearize the spectrum of the quasiparticles:

$$E(\mathbf{k}) = v |\sin[k_F(\mathbf{k})_x a]| q_{\parallel}(\mathbf{k}) \quad (6)$$

which is similar to Eq. (2) close to the Fermi surface. Here $q_{\parallel}(\mathbf{k}) \equiv (\mathbf{k} - \mathbf{k}_F(\mathbf{k})) \cdot \mathbf{k}_F(\mathbf{k})/|\mathbf{k}_F(\mathbf{k})|$, where $\mathbf{k}_F(\mathbf{k})$ is the wave-vector on the Fermi surface closest to \mathbf{k} , and $k_F(\mathbf{k})_x$ is the x -component of $\mathbf{k}_F(\mathbf{k})$.

The difficulty with bosonizing this Fermi surface is that at the four corners of the Fermi surface the Fermi velocities are zero and the Fermi surface normal vectors are not well-defined in the vicinity of the van Hove points. Below half-filling however the van Hove singularity is not encountered. So we introduce a model spectrum which simulates the Hubbard model near half-filling but with a smoothed out van Hove singularity. We modify the spectrum in Eq. (6) as following

$$\begin{aligned} E(\mathbf{k}) &= v |\sin[k_F(\mathbf{k})_x a]| q_{\parallel}(\mathbf{k}) , \quad \epsilon/a < |k_F(\mathbf{k})_x| < (\pi - \epsilon)/a , \\ &= v \sin(\epsilon a) q_{\parallel}(\mathbf{k}) , \quad \text{otherwise} \end{aligned} \quad (7)$$

and we smooth the four corners of the Fermi surface as four quarter-circles with a radius $\sqrt{2}\epsilon/a$ (Fig. 1). So we define the Fermi velocity function $v_F(\mathbf{k})$ as the coefficient of $q_{\parallel}(\mathbf{k})$ in Eq. (7). This choice is reasonable because the number of states near the van Hove points here are of order $\epsilon/\sin(\epsilon) \sim O(1)$, which is finite even if the limit $\epsilon \rightarrow 0$ is taken. This artificial smoothing simulates the van Hove singularity as the van Hove points accommodates a fixed fraction of the total number of states. From now on we set $1/a = 1$ and $v = 1$ for convenience. The factor $1/a$ may be recovered whenever a comparison with other momentum scales is needed. With this convention, for example, the nesting vectors are expressed as $\mathbf{Q} \equiv \pm(\pi, \pi)$ or $\pm(\pi, -\pi)$.

Now that the Fermi velocities are well-defined over the whole Fermi surface, the model may be bosonized. We coarse-grain the Fermi surface into small squat boxes of a width Λ along the Fermi surface and a height $\lambda(S) \equiv \varepsilon_c/v_F(S)$ normal to the Fermi surface, as shown in Fig. 1. Here $v_F(S)$ is the Fermi velocity function at the squat box S . Then we introduce a coarse-grained charge current which lives in a squat box labeled as S :

$$J_{\alpha}(\mathbf{k}_S; \mathbf{q}) = \sum_{\mathbf{k}} \theta(\mathbf{S}; \mathbf{k} - \mathbf{q}) \theta(\mathbf{S}; \mathbf{k}) \{ \psi_{\mathbf{k}-\mathbf{q}, \alpha}^{\dagger} \psi_{\mathbf{k}, \alpha} - \delta_{\mathbf{q}, \mathbf{0}} n_{\mathbf{k}, \alpha} \} . \quad (8)$$

Here $n_{\mathbf{k}, \alpha} = \langle \psi_{\mathbf{k}, \alpha}^{\dagger} \psi_{\mathbf{k}, \alpha} \rangle$. α is the spin index and the label S identifies a patch on the Fermi surface with a Fermi momentum \mathbf{k}_S and $\theta(\mathbf{S}; \mathbf{k}) = 1$ if \mathbf{k} lies inside a squat box centered on \mathbf{k}_S and $\theta(\mathbf{S}; \mathbf{k}) = 0$ otherwise. The two momentum scales $\Lambda, \lambda(S)$ are taken to be small so that $1/a \gg \Lambda \gg \lambda(S)$ at each Fermi surface patch. The latter inequality is needed to minimize scattering of fermions outside of the squat box so that the number of fermions in each patch on the Fermi surface is conserved. Now the limit of $\epsilon \rightarrow 0$ is not permitted since it violates the condition of $\epsilon/a \gg \Lambda$ at the four van Hove points. Instead, we take ϵ as a small non-zero number.

The $U(1)$ current algebra reads⁷⁻⁹

$$[J_{\alpha}(\mathbf{k}_S; \mathbf{q}), J_{\beta}(\mathbf{k}_T; \mathbf{p})] = \delta_{\alpha\beta} \delta_{S,T} \delta_{\mathbf{q}+\mathbf{p}, \mathbf{0}}^2 \Omega \mathbf{q} \cdot \hat{\mathbf{n}}_S , \quad (9)$$

which holds when $1/a \gg \Lambda \gg \lambda(S)$. Here $\Omega \equiv \Lambda(L/2\pi)^2$ is the number of states in the squat box divided by $\lambda(S)$ and $\hat{\mathbf{n}}_S$ is a unit vector normal to the Fermi surface at patch S . The algebra Eq. (9) makes it possible to bosonize the currents. The bosonic representation of the currents is

$$J_{\alpha}(\mathbf{k}_S; \mathbf{x}) = \sqrt{4\pi} \hat{\mathbf{n}}_S \cdot \nabla \phi_{\alpha}(\mathbf{k}_S; \mathbf{x}) , \quad (10)$$

where the bosonic fields ϕ_{α} satisfy the canonical commutation relations. Then the fermion quasiparticle fields at each patch can be expressed in terms of boson fields as⁸

$$\begin{aligned} \psi_{\alpha}(\mathbf{k}_S; \mathbf{x}, t) &\equiv e^{i\mathbf{k}_S \cdot \mathbf{x}} \sum_{\mathbf{p}} \theta(\mathbf{S}; \mathbf{p}) e^{i(\mathbf{p}-\mathbf{k}_S) \cdot \mathbf{x}} \psi_{\alpha\mathbf{p}}(t) \\ &= \sqrt{\frac{\Lambda\lambda(S)/2}{(2\pi)^2}} e^{i\mathbf{k}_S \cdot \mathbf{x}} \exp \left\{ i \frac{\sqrt{4\pi}}{\Omega} \phi_{\alpha}(\mathbf{k}_S; \mathbf{x}, t) \right\} \hat{O}(S) . \end{aligned} \quad (11)$$

Here $\hat{O}(S)$ is an ordering operator introduced to maintain Fermi statistics along the Fermi surface.

The bosonized effective action of the low-energy theory is

$$S = \sum_S \sum_{\mathbf{q}, \lambda(S) > \mathbf{q} \cdot \hat{\mathbf{n}}_S > 0} \int \frac{d\omega}{2\pi} [\omega - v_F(S) \mathbf{q} \cdot \hat{\mathbf{n}}_S] a^{*\alpha}(\mathbf{k}_S; q) a_\alpha(\mathbf{k}_S; q) + S_I. \quad (12)$$

Here S_I is the fermion interaction terms which we discuss later. The charge currents are related to the canonical boson operators a and a^\dagger by

$$J_\alpha(\mathbf{k}_S; \mathbf{q}) = \sqrt{\Omega |\mathbf{q} \cdot \hat{\mathbf{n}}_S|} [a_\alpha(\mathbf{k}_S; \mathbf{q}) \theta(\mathbf{q} \cdot \hat{\mathbf{n}}_S) + a_\alpha^\dagger(\mathbf{k}_S; -\mathbf{q}) \theta(-\mathbf{q} \cdot \hat{\mathbf{n}}_S)], \quad (13)$$

where

$$[a_\alpha(\mathbf{k}_S; \mathbf{q}), a_\beta^\dagger(\mathbf{k}_T; \mathbf{p})] = \delta_{\alpha\beta} \delta_{S,T} \delta_{\mathbf{p},\mathbf{q}}^2. \quad (14)$$

Here $\theta(x) = 1$ if $x > 0$ and $\theta(x) = 0$ otherwise. From Eq. (11) the fermion Greens function can be expressed in terms of the Fourier transformed boson correlation function and it is given by¹⁴

$$\begin{aligned} G_F^\alpha(\mathbf{k}_S; \mathbf{x}, t) &\equiv i \langle \psi^{\dagger\alpha}(\mathbf{k}_S; \mathbf{x}, t) \psi_\alpha(\mathbf{k}_S; \mathbf{0}, 0) \rangle \\ &= \frac{\lambda(S) \Lambda/2}{(2\pi)^2} e^{i\mathbf{k}_S \cdot \mathbf{x}} \exp \left[\int \frac{d^2 q}{(2\pi)^2} \int \frac{d\omega}{2\pi} [e^{i(\mathbf{q} \cdot \mathbf{x} - \omega t)} - 1] \right. \\ &\quad \left. \times \frac{(2\pi)^2}{\Lambda \mathbf{q} \cdot \hat{\mathbf{n}}_S} \langle a_\alpha(\mathbf{k}_S; \mathbf{q}) a_\alpha^\dagger(\mathbf{k}_S; \mathbf{q}) \rangle \right]. \end{aligned} \quad (15)$$

Next consider the renormalization of the fermion interactions. As in the case of a circular Fermi surface, the marginal interactions take the form of four-fermion (two-body) interactions, as can be verified by counting the engineering dimension. Unlike the case of a circular Fermi surface, however, many large-momentum scattering channels are now marginal due to the geometry of the nesting. Some of the channels give rise to the spin-density-wave (SDW) or charge-density-wave (CDW) instabilities. These logarithmically renormalized channels are discussed in Sec. IV. For now, the zero-sound (ZS) channel may be incorporated. This channel yields a Fermi liquid solution for a circular Fermi surface in two dimensions and a Luttinger liquid in one dimension. It is important to include this channel in the free action before the large momentum scattering channels are studied perturbatively. This permits a check on whether the Fermi surface breaks down in the presence of the ZS.

For simplicity, we suppress all momentum dependence in the coupling function and drop the spin indices. Inclusion of spin exchange channel does not change the result qualitatively. The ZS channel in the fermion basis is following:

$$S_{ZS} = - \int d^2 x dt F(S, T) \psi^\dagger(\mathbf{k}_S; \mathbf{x}, t) \psi(\mathbf{k}_S; \mathbf{x}, t) \psi^\dagger(\mathbf{k}_T; \mathbf{x}, t) \psi(\mathbf{k}_T; \mathbf{x}, t) \quad (16)$$

Note that a $U(1)$ phase rotation in each squat box $\psi(\mathbf{k}_S; \mathbf{x}, t) \rightarrow e^{i\Gamma(S)} \psi(\mathbf{k}_S; \mathbf{x}, t)$ and $\psi^\dagger(\mathbf{k}_S; \mathbf{x}, t) \rightarrow e^{-i\Gamma(S)} \psi^\dagger(\mathbf{k}_S; \mathbf{x}, t)$ leaves the action invariant. Physically, this infinite $U(1)$ symmetry means that the number of fermions at each patch on the Fermi surface is conserved. This channel can be expressed in terms of $U(1)$ currents since Eq. (8) is $U(1)$ invariant at each patch. The ZS channel in the bosonized form is succinctly written as

$$S_{ZS} = - \frac{1}{V} \sum_{S,T} \sum_{\mathbf{q}} \int \frac{d\omega}{2\pi} F(S, T) J(\mathbf{k}_S; q) J(\mathbf{k}_T; -q) \quad (17)$$

which is marginal since it is bilinear in bosons. Here q denotes (\mathbf{q}, ω) . The solution is a Gaussian boson parameterized by the shape of the Fermi surface and the coupling parameter $F(S, T)$. Those which do not have infinite $U(1)$ -symmetry are not expressed as bilinear in currents but they can be studied perturbatively. Here for simplicity the case $F(S, T) = F_0$ is studied.

Turning attention to the fermions on the nested part of the Fermi surface since that is where the most singular behavior may arise, we make use of the generating functional method,^{15,16} and obtain the boson correlation function,

$$\langle a(\mathbf{k}_S; q) a^\dagger(\mathbf{k}_S; q) \rangle = \frac{i}{\omega - v_F(S) \mathbf{q} \cdot \hat{\mathbf{n}}_S} + i \frac{\Lambda}{(2\pi)^2} \frac{\mathbf{q} \cdot \hat{\mathbf{n}}_S}{(\omega - v_F(S) \mathbf{q} \cdot \hat{\mathbf{n}}_S)^2} [K_0(q)]^{-1}, \quad (18)$$

and the fermion Greens function is given by Eq. (15). Here,

$$\begin{aligned} K_0(q) &= \frac{1}{F_0} - \frac{2\Lambda}{(2\pi)^2} \sum_S \frac{\theta(\mathbf{q} \cdot \hat{\mathbf{n}}_S) \mathbf{q} \cdot \hat{\mathbf{n}}_S}{\omega - v_F(S) \mathbf{q} \cdot \hat{\mathbf{n}}_S} \\ &= \frac{1}{F_0} + \frac{\sqrt{2}}{(2\pi)^2} \left[(2\pi)^2 \chi_0(\omega, \sin \epsilon \mathbf{q}) + \chi_N(\omega, \mathbf{q}) \right], \end{aligned} \quad (19)$$

where χ_N is the contribution from the nested part of the Fermi surface:

$$\begin{aligned}\chi_N(q) = & \frac{4}{\sqrt{1 - \omega^2/q_{\parallel}^2}} \ln \left[\frac{\sqrt{1 - \omega^2/q_{\parallel}^2} + \cos \epsilon}{\sqrt{1 - \omega^2/q_{\parallel}^2} - \cos \epsilon} \right] \\ & + \frac{4}{\sqrt{1 - \omega^2/q_{\perp}^2}} \ln \left[\frac{\sqrt{1 - \omega^2/q_{\perp}^2} + \cos \epsilon}{\sqrt{1 - \omega^2/q_{\perp}^2} - \cos \epsilon} \right].\end{aligned}\quad (20)$$

Again q_{\parallel} is the component of \mathbf{q} parallel with the Fermi surface normal and q_{\perp} is the perpendicular component. The contribution from the curved part of the Fermi surface (χ_0) in Eq. (19) gives a self-energy correction $\text{Im } \Sigma \sim \omega^2 \ln \omega$ as in a Fermi liquid system.¹⁴ We perturbatively estimate the imaginary part of the quasiparticle self-energy which originates from Eq. (20). The imaginary part of $\chi_N(q)$ arises when $|\omega| < |q_{\parallel}| \sin \epsilon$, or $|\omega| < |q_{\perp}| \sin \epsilon$. To second order in F_0 , the boson correlation function is expanded as

$$\begin{aligned}\langle a(\mathbf{k}_S; q) a^\dagger(\mathbf{k}_S; q) \rangle \approx & \frac{i}{\omega - v_F(S) \mathbf{q} \cdot \hat{\mathbf{n}}_S} \\ & + i \frac{\Lambda}{(2\pi)^2} \frac{\mathbf{q} \cdot \hat{\mathbf{n}}_S}{(\omega - v_F(S) \mathbf{q} \cdot \hat{\mathbf{n}}_S)^2} \left(F_0 - F_0^2 \frac{\sqrt{2}}{(2\pi)^2} \chi_N(q) \right)\end{aligned}\quad (21)$$

where χ_0 term is dropped. The first order term in F_0 renormalizes the Fermi velocity at the quasiparticle pole just as in the Fermi liquid case, but the velocity correction is $\delta v = F_0 \Lambda / k_F (2\pi)^2$, which is infinitesimal. Spin-charge velocity separation does not occur, as can be easily shown when the spin indices and the exchange channel are included in the effective action. Inserting Eq. (21) into Eq. (15), expanding the exponential to the second order in F_0 , and performing a Fourier transform into (\mathbf{k}, ω) space yields the imaginary correction to the quasiparticle self-energy.¹⁴ Then $\text{Im } \Sigma(\mathbf{k}, \omega) \propto \omega F_0^2 \Lambda / k_F$, which is of a marginal Fermi liquid form.¹⁷ Similarly, corrections of higher orders in F_0 can be estimated and we find that they also yield a marginal Fermi liquid form. This agrees with previous expectation by others who obtained the inverse lifetime of quasiparticles $1/\tau \sim T$ as a function of the temperature.⁶ Since the quasiparticle weight of a marginal Fermi liquid vanishes at the Fermi surface as the inverse of a logarithm, the Fermi liquid fixed point breaks down but the breakdown of the Fermi surface is smooth enough for the bosonization and the subsequent RG procedure to be applicable.¹⁶ Therefore we can confidently apply the RG method to analyze large-momentum channels which do not preserve the infinite $U(1)$ -symmetry.

One might wonder whether the marginal Fermi liquid like behavior of the nested fermion system has relevance to the linear- T in-plane resistivity of cuprate materials in the normal state.¹⁸ However, we only have considered a simplified single-band Hubbard model with the ZS channel alone whereas a three-band Hubbard model may be a better description of the cuprate materials. For example, we have not incorporated in the model the strong van Hove singularity which is present in the cuprate materials.¹⁹ Furthermore, the n -doped NCCO material exhibits T^2 -resistivity even though photoemission studies show a nested Fermi surface.²⁰ This suggests that nesting with the ZS alone is not sufficient to account for the behavior of the resistivity in the normal states of cuprate superconductors.

In the following sections, we study large-momentum scattering channels by the perturbative RG method. We do not explicitly include the ZS channel at the outset but we assume that it contributes sub-leading corrections to RG equations. For example, though bosons in different patches are correlated via the ZS, the correlation between fermions in different patches is negligible as following:

$$\langle \psi^\dagger(\mathbf{k}_S; \mathbf{x}) \psi(\mathbf{k}_T; \mathbf{0}) \rangle \propto \frac{1}{L} e^{\langle \phi(\mathbf{k}_S; \mathbf{x}) \phi(\mathbf{k}_T; \mathbf{0}) \rangle} \rightarrow 0, \quad (22)$$

where L is the system size.¹⁴ Also the self-energy corrections are of order $\Lambda a \ll 1$ times smaller than the leading order. So the leading RG equations we obtain in the following sections are assumed to be unchanged even if the ZS channel is considered.

III. RG OF THE BCS CHANNEL

In this section we study the RG flow of the BCS channel for the nested Fermi surface and find an analog of Landau theorem. As for the case of an isotropic circular Fermi surface, the BCS channel in a nested square Fermi surface flows logarithmically in scale length since the Fermi surface is symmetric under reflection at the origin in the momentum space. On a circular Fermi surface, Landau theorem²¹ states that there occurs a BCS instability if

any one value of V_l is negative where V_l is the l th orbital angular momentum component of the BCS vertex function $V(\theta_1, \theta_2) = \sum_l e^{il(\theta_1 - \theta_2)} V_l$. Here θ_1, θ_2 are the angular variables on the Fermi surface in the momentum space. This theorem can be seen in the RG equation for V_l derived by Shankar,^{11,14}

$$\frac{dV_l}{d \ln s} = - \frac{1}{2\pi} V_l^2, \quad (23)$$

the solution of which is

$$V_l(s) = \frac{V_l}{1 + \frac{V_l}{2\pi} \ln s}, \quad (24)$$

for each l . Thus, if any $V_l < 0$, it eventually leads to instability.

In case of the nested Fermi surface there is no rotational invariance in the BCS vertex function, so $V(\mathbf{k}_S, \mathbf{k}_T)$ must be expanded in a double Fourier series.³ Consequently the Fourier coefficients are coupled in the resulting RG equations, unlike in the case of a circular Fermi surface. First we discuss the possible symmetry of the order parameter in a square lattice. The BCS vertex function has D_4 symmetry and there are five sets of basis functions which generate the two-dimensional function space to which the vertex function belongs. The five sets are represented as A_1 and A_2 (s -wave), B_1 and B_2 (d -wave), and E (p -wave).³ The basis functions in each set are following:

$$\begin{aligned} A_1 : & \cos 2nk_x \\ A_2 : & \text{sgn}(k_y) \sin 2nk_x \\ B_1 : & \cos(2n+1)k_x \\ B_2 : & \text{sgn}(k_y) \sin(2n+1)k_x \\ E : & a \sin(n+1/2)k_x + b \text{sgn}(k_y) \cos(n+1/2)k_x, \end{aligned} \quad (25)$$

where we have parameterized the basis functions with k_x and the sign of k_y on the square Fermi surface which is defined by $\cos k_x + \cos k_y = 0$. In general the BCS vertex function on a square lattice can be expressed as a double Fourier expansion in terms of these basis functions. Due to the D_4 symmetry of the BCS vertex function, the expansion does not contain crossed terms between basis functions of different symmetry sets, so the five sets are decoupled from one another in the RG equation at the outset.

Now we inspect the RG equation of the BCS obtained in bosonization language,¹⁴

$$\frac{dV(\mathbf{k}_S, \mathbf{k}_T)}{d(\ln s)} = - \frac{\Lambda}{(2\pi)^2} \sum_U \frac{1}{v_F(U)} V(\mathbf{k}_S, \mathbf{k}_U) V(\mathbf{k}_U, \mathbf{k}_T). \quad (26)$$

Notice that there is a weight function of $1/v_F(U)$ in the sum. To analyze the RG equation, we modify the basis functions in Eq. (25) so that they are orthonormal under summation over the Fermi surface with the weight function $1/v_F(U)$. The modified basis functions are given by

$$\begin{aligned} a_1(n, \mathbf{k}) &\equiv \left[\frac{v_F(\mathbf{k})}{2\pi\sqrt{2}} \right]^{1/2} \cos 2nk_x, \quad a_1(0, \mathbf{k}) \equiv \left[\frac{v_F(\mathbf{k})}{4\pi\sqrt{2}} \right]^{1/2} \\ a_2(n, \mathbf{k}) &\equiv \text{sgn}(k_y) \left[\frac{v_F(\mathbf{k})}{2\pi\sqrt{2}} \right]^{1/2} \sin 2nk_x \\ b_1(n, \mathbf{k}) &\equiv \left[\frac{v_F(\mathbf{k})}{2\pi\sqrt{2}} \right]^{1/2} \cos(2n+1)k_x \\ b_2(n, \mathbf{k}) &\equiv \text{sgn}(k_y) \left[\frac{v_F(\mathbf{k})}{2\pi\sqrt{2}} \right]^{1/2} \sin(2n+1)k_x \\ e(n, \mathbf{k}) &\equiv \left[\frac{v_F(\mathbf{k})}{2\pi\sqrt{2}} \right]^{1/2} [c_1 \sin(n+1/2)k_x + c_2 \text{sgn}(k_y) \cos(n+1/2)k_x]. \end{aligned} \quad (27)$$

The BCS vertex function can be expanded as

$$\begin{aligned} V(\mathbf{k}_S, \mathbf{k}_T) = \sum_{n,m} \big\{ & C_1^{nm} a_1(n, \mathbf{k}_S) a_1(m, \mathbf{k}_T) + C_2^{nm} a_2(n, \mathbf{k}_S) a_2(m, \mathbf{k}_T) \\ & + C_3^{nm} b_1(n, \mathbf{k}_S) b_1(m, \mathbf{k}_T) + C_4^{nm} b_2(n, \mathbf{k}_S) b_2(m, \mathbf{k}_T) \\ & + C_5^{nm} e(n, \mathbf{k}_S) e(m, \mathbf{k}_T) \big\} \end{aligned} \quad (28)$$

This expansion is valid as long as $\min(|v_F(\mathbf{k})|) > 0$ which holds in the model considered here. In fact, $\min(|v_F(\mathbf{k})|)$ is zero only at exactly half-filling.

Now insert Eq. (28) into Eq. (26) to obtain the RG equations of Fourier coefficients:

$$\frac{dC_i^{nm}}{d \ln s} = - \frac{1}{(2\pi)^2} \sum_{l=0}^{\infty} C_i^{nl} C_i^{lm} \quad (29)$$

where $i = 1, \dots, 5$. Now the analog of Landau theorem in the nested fermion liquid can be obtained. Namely, the diagonal Fourier coefficients obey the following equations,

$$\frac{dC_i^{nn}}{d \ln s} = - \frac{1}{(2\pi)^2} \sum_{l=0}^{\infty} |C_i^{nl}|^2. \quad (30)$$

Here the diagonal coefficients decrease as the length scale increases. Thus if any one value of C_i^{nn} starts out negative, a BCS instability occurs. This is similar to the Landau theorem in an isotropic circular Fermi surface. This criterion of instability permits us to identify the possible symmetry of the resulting order parameter, since the gap function is related to the BCS vertex function by the following:

$$\Delta_{\mathbf{k}} = - \sum_{\mathbf{k}'} V(\mathbf{k}, \mathbf{k}') \frac{\Delta_{\mathbf{k}'}}{2E(\mathbf{k}')} , \quad (31)$$

where \mathbf{k}, \mathbf{k}' are within the thin shell around the Fermi surface and $E(\mathbf{k}')$ is the spectrum of the low-lying excitation in the superconducting state. In the next section we apply this result to search for a possible BCS instability in the presence of a repulsive interaction.

IV. RG OF REPULSIVE INTERACTIONS

In this section we discuss the RG flow of repulsive interactions. We only consider those channels which flow logarithmically in length scale s . To simplify the analysis we take coupling functions to be independent of momentum.

There are three classes of interaction channels which are logarithmically renormalized in the presence of nesting. The first class is the CDW or SDW channel. In case of a repulsive bare Hubbard interaction, it is the SDW channel that leads to an instability. This channel is shown to have little overlap with the BCS channel and is practically decoupled from the BCS. The second and third classes are $Q = 0$ and $Q = 2k_F$ repulsive (or AF exchange) channels which renormalize the BCS channel. In the following two subsections we study the RG equation in the SDW (CDW) channel and in the other repulsive (or AF) channel which renormalize the BCS and calculate the Kohn-Luttinger effect.

A. CDW and SDW channels

In this subsection we derive the RG flows of density-wave channels, which have negligible overlap with the BCS channel. The channel is:

$$S_{DW} = \int d^2x \, dt \, \frac{F_{DW}}{2} \sum_{S,T} \sum_i \psi^{\dagger\alpha}(\mathbf{k}_S; x) \, \psi_{\beta}(\mathbf{k}_S + \mathbf{Q}_i; x) \\ \times \psi^{\dagger\gamma}(\mathbf{k}_T; x) \, \psi_{\delta}(\mathbf{k}_T + \mathbf{Q}_j; x) \, [\delta_{\alpha}^{\beta} \delta_{\gamma}^{\delta} - \delta_{\gamma}^{\beta} \delta_{\alpha}^{\delta}] . \quad (32)$$

Here $\mathbf{Q}_i, \mathbf{Q}_j$ are two of the four nesting vectors. (Fig. 2). Due to the nesting, this channel flows logarithmically in scale length and causes a CDW or a SDW instability, depending on the sign of F_{DW} . The spin indices in Eq. (32) are appropriately symmetrized according to the Fermi statistics.¹³ Separating the interaction F_{DW} into decoupled CDW and SDW channels,

$$S_{DW} = \frac{1}{2} \int d^2x \, dt \, \sum_{S,T} \{ F_{SDW} \, \mathbf{S}_Q(S; x) \cdot \mathbf{S}_Q(T; x) + F_{CDW} \, n_Q(S; \mathbf{x}) \, n_Q(T; \mathbf{x}) \} \quad (33)$$

where

$$\mathbf{S}_Q(S; \mathbf{x}) = \frac{1}{2} \psi^{\dagger\alpha}(\mathbf{k}_S; \mathbf{x}) \sigma_\alpha^\beta \psi_\beta(\mathbf{k}_S + \mathbf{Q}; \mathbf{x}) \quad (34)$$

and

$$n_Q(S; \mathbf{x}) = \psi^{\dagger\alpha}(\mathbf{k}_S; \mathbf{x}) \psi_\alpha(\mathbf{k}_S + \mathbf{Q}; \mathbf{x}) \quad (35)$$

are the spin-density and the charge-density respectively. The primed summation over S, T indicates that the sum is over the nested parts of the Fermi surface. First, we investigate the RG flow of the CDW term. For simplicity we drop the spin indices. From Eq. (11) the bosonized form of the CDW action is as follows

$$\begin{aligned} S_{CDW} &= \frac{1}{2} \sum'_{S,T} \int dt d^2x F_{CDW}(S, T) \psi^\dagger(\mathbf{k}_S; x) \psi(\mathbf{k}_S + \mathbf{Q}_i; x) \psi^\dagger(\mathbf{k}_T; x) \psi(\mathbf{k}_T + \mathbf{Q}_j; x) \\ &= \frac{1}{2} \left(\frac{\Lambda}{(2\pi)^2} \right)^2 \sum'_{S,T} \int dt d^2x F_{CDW}(S, T) \frac{\lambda(S) \lambda(T)}{4} \\ &\quad \times \exp \left\{ i \frac{\sqrt{4\pi}}{\Omega} [\phi(\mathbf{k}_S + \mathbf{Q}_i; x) + \phi(\mathbf{k}_T + \mathbf{Q}_j; x) - \phi(\mathbf{k}_S; x) - \phi(\mathbf{k}_T; x)] \right\}. \end{aligned} \quad (36)$$

where x denotes (\mathbf{x}, t) . The scaling of ε_c , x , t follows

$$t \rightarrow t'/s, \quad x_{\parallel} \rightarrow x'_{\parallel}/s, \quad \varepsilon_c \rightarrow s\varepsilon'_c \quad (37)$$

where s is the scale of the length. Dimensional analysis shows that S_{CDW} is scale-invariant and thus marginal.

Next the fields may be split into higher and lower energy modes $\phi(\mathbf{k}_S; x) \rightarrow \phi'(\mathbf{k}_S; x) + h(\mathbf{k}_S; x)$ where h is the field of higher energy modes whose momentum ranges $\lambda'(S)/2 < |\mathbf{p}| < \lambda(S)/2$ where $\lambda'(S) \equiv \varepsilon'_c/v_F(S)$. The equal-time correlation function of h fields is following:

$$\begin{aligned} \langle h(\mathbf{k}_S; \mathbf{x}) h(\mathbf{k}_T; \mathbf{0}) \rangle &= \delta_{S,T} \frac{\Omega^2}{4\pi} \ln \left(\frac{\hat{\mathbf{n}}_S \cdot \mathbf{x} + 2is/\lambda(S)}{\hat{\mathbf{n}}_S \cdot \mathbf{x} + 2i/\lambda(S)} \right); \quad |\hat{\mathbf{n}}_S \times \mathbf{x}| \ll 1 \\ &= 0; \quad |\hat{\mathbf{n}}_S \times \mathbf{x}| \gg 1 \end{aligned} \quad (38)$$

We study how the partition function is renormalized after the fast momentum modes are integrated out.

$$\begin{aligned} \langle e^{-S_{CDW}} \rangle &= \langle 1 - S_{CDW} + \frac{1}{2} S_{CDW}^2 + \dots \rangle \\ &= \exp \left[-S'_{CDW} \right]. \end{aligned} \quad (39)$$

Here the average in the bracket is taken only over the high-energy fields h and S'_{CDW} is the renormalized CDW action. The third term in the r.h.s. of Eq. (39) gives the second order in F_{CDW} correction to S_{CDW} . Using the formula $\langle e^A e^B \rangle = e^{\langle AB + (A^2 + B^2)/2 \rangle}$ and Eq. (38), we obtain

$$\begin{aligned} \frac{1}{2} [\langle S_{CDW}^2 \rangle - \langle S_{CDW} \rangle^2] &= \frac{1}{2} \left[\frac{\Lambda}{(2\pi)^2} \right]^4 \sum'_{S,T,U} \int dt d^2x F_{CDW}^2 \frac{\lambda(S) \lambda(T) \lambda^2(U)}{16s^4} \\ &\quad \times \exp \left\{ i \frac{\sqrt{4\pi}}{\Omega} [\phi(\mathbf{k}_S + \mathbf{Q}_i; x) + \phi(\mathbf{k}_T + \mathbf{Q}_j; x) - \phi(\mathbf{k}_S; x) - \phi(\mathbf{k}_T; x)] \right\} \\ &\quad \times \int du d^2y \exp \left\{ \frac{4\pi}{\Omega^2} [\langle h(\mathbf{k}_U; \mathbf{y}, u) h(\mathbf{k}_U; \mathbf{0}, u) \rangle + \langle h(\mathbf{k}_U + \mathbf{Q}_i; \mathbf{y}, u) h(\mathbf{k}_U + \mathbf{Q}_i; \mathbf{0}, u) \rangle] \right\} \\ &\quad + \text{subleading terms} \\ &\approx \frac{1}{2} \left[\frac{\Lambda}{(2\pi)^2} \right]^4 \sum'_{S,T} \int dt d^2x \sum_U F_{CDW}^2 \frac{\lambda^2(U)}{4s^2} \frac{2\pi}{\Lambda} \int du d(\hat{\mathbf{n}}_U \cdot \mathbf{y}) \frac{4s^2/\lambda(U)^2}{[v_F(U)u]^2 + (\hat{\mathbf{n}}_U \cdot \mathbf{y})^2} \\ &\quad \times \frac{\lambda(S) \lambda(T)}{4s^2} \exp \left\{ i \frac{\sqrt{4\pi}}{\Omega} [\phi(\mathbf{k}_S + \mathbf{Q}_i; x) + \phi(\mathbf{k}_T + \mathbf{Q}_j; x) - \phi(\mathbf{k}_S; x) - \phi(\mathbf{k}_T; x)] \right\} \\ &\quad + \text{subleading terms} \end{aligned} \quad (40)$$

Here $v_F(U)$ denotes the Fermi velocity at the patch U . Replacing $\lambda(S)$ with $s\lambda'(S)$ ($\lambda'(S)$ is the new cutoff) and performing the integrals over $\hat{\mathbf{n}}_U \cdot \mathbf{y}$ and u , we extract the correction to the CDW coupling function

$$\frac{dF_{CDW}(s)}{d\ln(s)} = -\frac{\Lambda}{2(2\pi)^2} \sum_U' \frac{1}{v_F(U)} F_{CDW}^2. \quad (41)$$

Therefore, we expect instability in this channel if F_{CDW} is strictly negative. This agrees with the result obtained by Shankar.¹¹ $F_{CDW} < 0$ corresponds to a bare attractive interaction ($U < 0$) and the CDW instability leads to the phase transition into a charge-density ordering with the period (π, π) and $(\pi, -\pi)$.

Likewise, a similar RG transformation can be performed to obtain the flow equation for the SDW channel:

$$S_{SDW} = -\frac{1}{2} \int d^2x dt \sum_{S,T}' F_{SDW} \mathbf{S}_Q(S; x) \cdot \mathbf{S}_Q(T; x) \quad (42)$$

yielding:

$$\frac{dF_{SDW}(s)}{d\ln(s)} = -\frac{\Lambda}{(2\pi)^2} \sum_U' \frac{1}{v_F(U)} F_{SDW}^2 \quad (43)$$

As expected there occurs an instability when $F_{SDW} < 0$, which corresponds to a bare repulsive interaction ($U > 0$). The SDW instability leads to the AF spin-density ordering with the period (π, π) and $(\pi, -\pi)$ since the on-site repulsive interaction induces an AF exchange interaction with the nearest neighbors.

Since the RG equation for the BCS channel is of interest, we now discuss the overlap between the BCS and the SDW (CDW) channels. In Fig. 3 we show a typical scattering channel which belongs to both the BCS and the density-wave channel. In terms of the BCS, it can be written as

$$S_{\text{overlap}} = \sum_{S,T} \int d^2x dt V(\mathbf{k}_S, \mathbf{k}_T) \psi^{\dagger\alpha}(\mathbf{k}_S; x) \psi^{\dagger\beta}(-\mathbf{k}_S; x) \\ \times \psi_\beta(-\mathbf{k}_T; x) \psi_\alpha(\mathbf{k}_T; x) \delta_{\mathbf{k}_T, \mathbf{k}_S + \mathbf{Q}}. \quad (44)$$

Obviously there is a severe phase space restriction due to the factor of $\delta_{\mathbf{k}_T, \mathbf{k}_S + \mathbf{Q}}$ in the overlapped channel, which amounts to a factor of $\Lambda a \ll 1$. Therefore, the SDW (CDW) is practically decoupled from the BCS channel. The renormalization of the BCS comes exclusively from the other repulsive or AF exchange channels which we discuss in the next subsection. Here we can evaluate the energy scale of the SDW instability for the future reference. From Eq. (43), we obtain the critical energy at which the SDW instability occurs:

$$E_{SDW} \sim E_F \exp \left[-\frac{1}{\frac{8\sqrt{2}}{(2\pi)^2} \ln \frac{2}{\epsilon} |F_{SDW}|} \right]. \quad (45)$$

B. Kohn-Luttinger effect

The two classes of repulsive channels which renormalize the BCS are shown in Fig. 4 and Fig. 5 and given by

$$S_R = \frac{1}{2} \sum_{S,T} \sum_{\Delta \mathbf{p}} \int d^2x dt F_R \psi^{\dagger\alpha}(\mathbf{k}_S; x) \psi_\beta(\mathbf{k}_S + \Delta \mathbf{p} + \mathbf{Q}_i; x) \\ \times \psi^{\dagger\gamma}(\mathbf{k}_T; x) \psi_\delta(\mathbf{k}_T - \Delta \mathbf{p} - \mathbf{Q}_i; x) [\delta_\alpha^\beta \delta_\gamma^\delta - \delta_\gamma^\beta \delta_\alpha^\delta], \quad (46)$$

which is the zero momentum process (Fig. 4) and

$$S_U = \frac{1}{2} \sum_{S,T} \sum_{\Delta \mathbf{p}} \int d^2x dt F_U \psi^{\dagger\alpha}(\mathbf{k}_S; x) \psi_\beta(\mathbf{k}_S + \Delta \mathbf{p} + \mathbf{Q}_i; x) \\ \times \psi^{\dagger\gamma}(\mathbf{k}_T; x) \psi_\delta(\mathbf{k}_T - \Delta \mathbf{p} + \mathbf{Q}_i; x) [\delta_\alpha^\beta \delta_\gamma^\delta - \delta_\gamma^\beta \delta_\alpha^\delta], \quad (47)$$

which is the $2k_F = Q$ process allowed because $2Q$ is a commensurate wave-vector (Fig. 5). In both channels we take the coupling functions to be momentum-independent and the spin indices are anti-symmetrized.¹³

Now we expand the partition function to the second order in $S_R + S_U$ and integrate out the high-energy modes and study the resulting effective action generated by this procedure. In the course of this RG procedure, S_R and S_U are renormalized as well as the BCS channel so the resulting flow equation will be a complicated set of coupled differential equations. We do not attempt to perform a complete analysis of the flow equations but we are only interested in the trend of initial growth of the BCS channel; the higher order coupled equations are important only in the very long length scale. Thus we only study how $S_R + S_U$ renormalizes the BCS in the initial stages of the growth near $s = 1$. The second order correction to the BCS is calculated in the same manner as in the previous subsection:

$$\begin{aligned} \frac{1}{2} \langle (S_R + S_U)^2 \rangle &\approx \ln s (F_R^2 + 4 F_U^2) \sum_S \sum_{\Delta \mathbf{p}} \int d^2x dt \psi^{\dagger\alpha}(\mathbf{k}_S; x) \psi^{\dagger\beta}(-\mathbf{k}_S; x) \\ &\quad \times \psi_\beta(\mathbf{k}_S + \Delta \mathbf{p} + \mathbf{Q}; x) \psi_\alpha(-\mathbf{k}_S - \Delta \mathbf{p} - \mathbf{Q}; x) \\ &\quad \times \frac{\sqrt{2}}{2(2\pi)^2} \frac{1}{\cos \Delta p/2} \ln \left(\frac{1 + \cos(\epsilon + |\Delta p|/2)}{1 - \cos(\epsilon + |\Delta p|/2)} \right) \\ &\quad + \frac{\ln s}{2} F_R^2 \sum_{S,T} \left[\frac{\sqrt{2}}{(2\pi)^2} \ln \left(\frac{1 + \cos \epsilon}{1 - \cos \epsilon} \right) + \frac{1}{2\pi} \right] \\ &\quad \times \int d^2x dt \psi^{\dagger\alpha}(\mathbf{k}_S; x) \psi^{\dagger\beta}(-\mathbf{k}_S; x) \psi_\beta(-\mathbf{k}_T; x) \psi_\alpha(\mathbf{k}_T; x) \\ &\quad + \text{non - BCS terms} . \end{aligned} \quad (48)$$

The second term in Eq. (48) contributes to the s -wave BCS channel. Since it is repulsive even in the first order to begin with, the s -wave BCS channel is not a candidate for instability. The first term in Eq. (48) gives RG flow to all BCS symmetry channels since it has a strong wave-vector dependence. More succinctly, the RG equation of the BCS channel is given by

$$\begin{aligned} \frac{dV_{BCS}(\mathbf{k}_S, \mathbf{k}_T)}{d \ln s} &= (F_R^2 + 4 F_U^2) \frac{\sqrt{2}}{2(2\pi)^2} \frac{1}{\cos \Delta p(S, T)/2} \ln \left(\frac{1 + \cos(\epsilon + |\Delta p(S, T)|/2)}{1 - \cos(\epsilon + |\Delta p(S, T)|/2)} \right) \\ &\quad - \frac{\Lambda}{(2\pi)^2} \sum_U \frac{1}{v_F(U)} V_{BCS}(\mathbf{k}_S, \mathbf{k}_U) V_{BCS}(\mathbf{k}_U, \mathbf{k}_T) , \end{aligned} \quad (49)$$

if S and T are in the same quadrant on the Fermi surface. When S and T are in different quadrants,

$$\frac{dV_{BCS}(\mathbf{k}_S, \mathbf{k}_T)}{d \ln s} = - \frac{\Lambda}{(2\pi)^2} \sum_U \frac{1}{v_F(U)} V_{BCS}(\mathbf{k}_S, \mathbf{k}_U) V_{BCS}(\mathbf{k}_U, \mathbf{k}_T) . \quad (50)$$

$\Delta p(S, T)$ is a vector along the nested Fermi surface which is shown in Fig. 4. For instance, $\Delta p(S, T) = |(\mathbf{k}_S - \mathbf{k}_T) \cdot \hat{\mathbf{x}} - \pi|$ if \mathbf{k}_S and \mathbf{k}_T are both in the first quadrant on the (k_x, k_y) plane. The expression of $\Delta p(S, T)$ in the other quadrants can be obtained by inverting the signs of \mathbf{k}_S or \mathbf{k}_T appropriately.

Now we are ready to check which symmetry channels are attractive by evaluating the generalized Fourier coefficients of the double expansion shown in Sec. III. Among the basis functions we introduced in Eq. (27), we especially focus on the fundamental modes whose Fourier coefficients are presumably the most significant. After performing the generalized Fourier transform of the r.h.s. of Eq. (49) we find that there are two diagonal Fourier coefficients which flow to negative numbers among the fundamental modes. Their rate of change is evaluated as following:

$$\begin{aligned} \frac{dC_2^{11}}{d \ln s} &= \Lambda^2 \sum_{S,T} \frac{1}{v_F(\mathbf{k}_S) v_F(\mathbf{k}_T)} \frac{dV_{BCS}(\mathbf{k}_S, \mathbf{k}_T)}{d \ln s} a_2(1, \mathbf{k}_S) a_2(1, \mathbf{k}_T) \\ &\approx -0.7 (F_R^2 + 4 F_U^2) - |C_2^{11}|^2 / (2\pi)^2 \end{aligned} \quad (51)$$

$$\begin{aligned} \frac{dC_3^{00}}{d \ln s} &= \Lambda^2 \sum_{S,T} \frac{1}{v_F(\mathbf{k}_S) v_F(\mathbf{k}_T)} \frac{dV_{BCS}(\mathbf{k}_S, \mathbf{k}_T)}{d \ln s} b_1(0, \mathbf{k}_S) b_1(0, \mathbf{k}_T) \\ &\approx -0.2 (F_R^2 + 4 F_U^2) - |C_3^{00}|^2 / (2\pi)^2 , \end{aligned} \quad (52)$$

where $C_2^{11}(s = 1) = C_3^{00}(s = 1) = 0$ initially. These are evaluated when $\epsilon \approx 0.1$. Here we find that the inequality $\left| \frac{dC_3^{00}}{d \ln s} \right| > \left| \frac{dC_2^{11}}{d \ln s} \right|$ holds for a sufficiently small ϵ . From Landau theorem we can infer that there can be a BCS

instability in either B_1 ($d_{x^2-y^2}$ -wave) or A_2 (eight-lobed s -wave) channel as long as the SDW instability does not set in. Furthermore, we can infer from the inequality $|\frac{dC_3^{00}}{d \ln s}| > |\frac{dC_2^{11}}{d \ln s}|$ that for a small enough ϵ , $d_{x^2-y^2}$ -wave superconductivity is preferred. The reason the inequality holds is that the $d_{x^2-y^2}$ -wave basis function $b_1(0, \mathbf{k})$ has bigger overlap than $a_2(1, \mathbf{k})$ does with the density of states at the Fermi surface which peaks at the van Hove points.

Of course, the $d_{x^2-y^2}$ -wave superconductivity is not the only possible ground state near half-filling. There is competition between the SDW and the BCS since both are favored in the presence of a bare on-site repulsive interaction. Slightly below half-filling, the nesting is not perfect but nevertheless effective as long as the effective theory around the Fermi surface covers a significant part of the nested Fermi surface. As the energy cutoff around the Fermi surface is reduced via RG towards ε_δ , where ε_δ is the energy deviation of the actual Fermi surface from the nested one, the SDW and AF exchange channel stop flowing whereas the BCS continues to be renormalized logarithmically as its flow is independent of nesting.¹¹ If initially the SDW coupling is small enough or if ε_δ is big enough so that it does not develop instability until $\varepsilon_c \rightarrow \varepsilon_\delta$, or $E_{SDW} < \varepsilon_\delta$, there never occurs a SDW instability. Although it is difficult to compute the critical energy, the BCS instability eventually sets in at a sufficiently low energy scale. From the argument above, the superconducting order parameter presumably has a $d_{x^2-y^2}$ -wave symmetry. This result is consistent with the expectation that AF exchange channel is conducive to $d_{x^2-y^2}$ -wave superconductivity and qualitatively in good agreement with the parquet solution obtained for a flat Fermi surface.²²

V. SUMMARY AND CONCLUSIONS

In this paper we investigated the BCS instability in a nested Fermion liquid with a bare repulsive interaction. When the ZS channel was incorporated we found that the low-energy fixed point was of a marginal Fermi liquid type. Although the Fermi liquid state broke down, multidimensional bosonization was still applicable. Large-momentum scattering channels were then included via the perturbative RG procedure in the boson basis. Among the logarithmically renormalized channels, the SDW showed the quickest flow due to the nesting, but it had negligible overlap with the BCS channel. The other repulsive or AF channels gave rise to a renormalization of the BCS couplings. We found that the $d_{x^2-y^2}$ -wave channel was rendered the most attractive. Close to but less than half-filling, when no instabilities develop in the SDW channel ($E_{SDW} < \varepsilon_\delta$), a $d_{x^2-y^2}$ -wave BCS instability sets in at sufficiently low temperatures. This is in agreement with the expectations of Monthoux, Balatsky, and Pines,⁵ and the result obtained by Zhelenyak, Yakovenko, and Dzyaloshinskii.²²

The procedure presented in this paper is useful for extracting information about the low-energy fixed points of lattice systems. Once a realistic band structure of the system near the Fermi surface is given as the input, one can analyze the phase structure and the order parameter symmetry at low temperatures. As regards the cuprate superconductors, it would be interesting to study the RG of a three-band Hubbard model. For detailed examination of the low-temperature phase structure of the materials, numerical works on the RG equation are needed. In this manner, one may be able to construct a phase diagram as a function of temperature and the filling factor (or doping).

ACKNOWLEDGEMENTS

The author thanks Youngjai Kiem, Brad Marston, and Jaejun Yu for helpful comments and discussions, and in particular, Brad Marston for careful reading of the manuscript.

* Present address: Na-207 Han-In APT, 517-3 Sutaek-dong, Kuri-shi Kyonggi-do, SEOUL KOREA
hjk@yollabolly.physics.brown.edu

¹ P. W. Anderson, Phys. Rev. Lett. **64**, 1839 (1990).

² W. Kohn and J. M. Luttinger, Phys. Rev. Lett. **15**, 524 (1965).

³ M. A. Baranov, A. V. Chubukov, and M. Yu Kagan, Int. J. of Mod. Phys. B **6**, 2471 (1992).

⁴ Andrey V. Chubukov, Phys. Rev. B **48**, 1097 (1993).

⁵ P. Monthoux, A. V. Balatsky, and D. Pines, Phys. Rev. Lett. **67**, 3448 (1991).

⁶ A. Virosztek and J. Ruvalds, Phys. Rev. B **42**, 4064 (1990).

- ⁷ F. D. M. Haldane, in *Luttinger's Theorem and Bosonization of the Fermi Surface*, Proceedings of the International School of Physics "Enrico Fermi," Course CXXI, Varenna, 1992, edited by R. Schrieffer and R. A. Broglia (North-Holland, New York, NY 1994).
- ⁸ A. Houghton and J. B. Marston, Phys. Rev. B **48**, 7790 (1993).
- ⁹ A. H. Castro-Neto and Eduardo H. Fradkin, Phys. Rev. Lett. **72**, 1393 (1994).
- ¹⁰ P. Kopietz, J. Hermisson, and K. Schönhammer, Phys. Rev. B **52**, 10877 (1995).
- ¹¹ R. Shankar, Rev. Mod. Phys. **66**, 129 (1994).
- ¹² R. Shankar, Physica A **177**, 530 (1991).
- ¹³ Gennady Y. Chitov and David Sénéchal, Phys. Rev. B **52**, 13487 (1995).
- ¹⁴ A. Houghton, H.-J. Kwon, and J. B. Marston, Phys. Rev. B **50**, 1351 (1994).
- ¹⁵ H.-J. Kwon, A. Houghton, and J. B. Marston, Phys. Rev. Lett. **73** 284 (1994).
- ¹⁶ H.-J. Kwon, A. Houghton, and J. B. Marston, Phys. Rev. B **52**, 8002 (1995).
- ¹⁷ C. M. Varma, I. B. Littlewood, and S. Schmitt-Rink, Phys. Rev. Lett. **63**, 1996 (1989).
- ¹⁸ See, for example, H. Takagi *et al.*, Phys. Rev. Lett. **69**, 2975 (1992).
- ¹⁹ D. S. Dessau *et al.*, Phys. Rev. Lett. **71**, 2781 (1993).
- ²⁰ D. M. King *et al.*, Phys. Rev. Lett. **70**, 3159 (1993).
- ²¹ E. M. Lifshitz and L. P. Pitaevskii, *Statistical Physics*, part 2 (Pergamon, New York, 1980).
- ²² Anatoley T. Zheleznyak, Victor M. Yakovenko, and Igor E. Dzyaloshinskii, "Parquet solution for a flat Fermi surface," cond-mat/9609118.

FIG. 1. The low-energy effective theory in the vicinity of the Fermi surface. The thin momentum shell is coarse-grained into squat boxes of a height λ and a width Λ . \mathbf{Q} is the nesting vector.

FIG. 2. A typical density-wave scattering channel.

FIG. 3. A typical overlap between density-wave and BCS channel.

FIG. 4. The repulsive or AF channels with a zero momentum transfer which logarithmically renormalize BCS channel.

FIG. 5. The repulsive or AF channels with a momentum transfer $2\mathbf{Q}$ which logarithmically renormalize BCS channel.

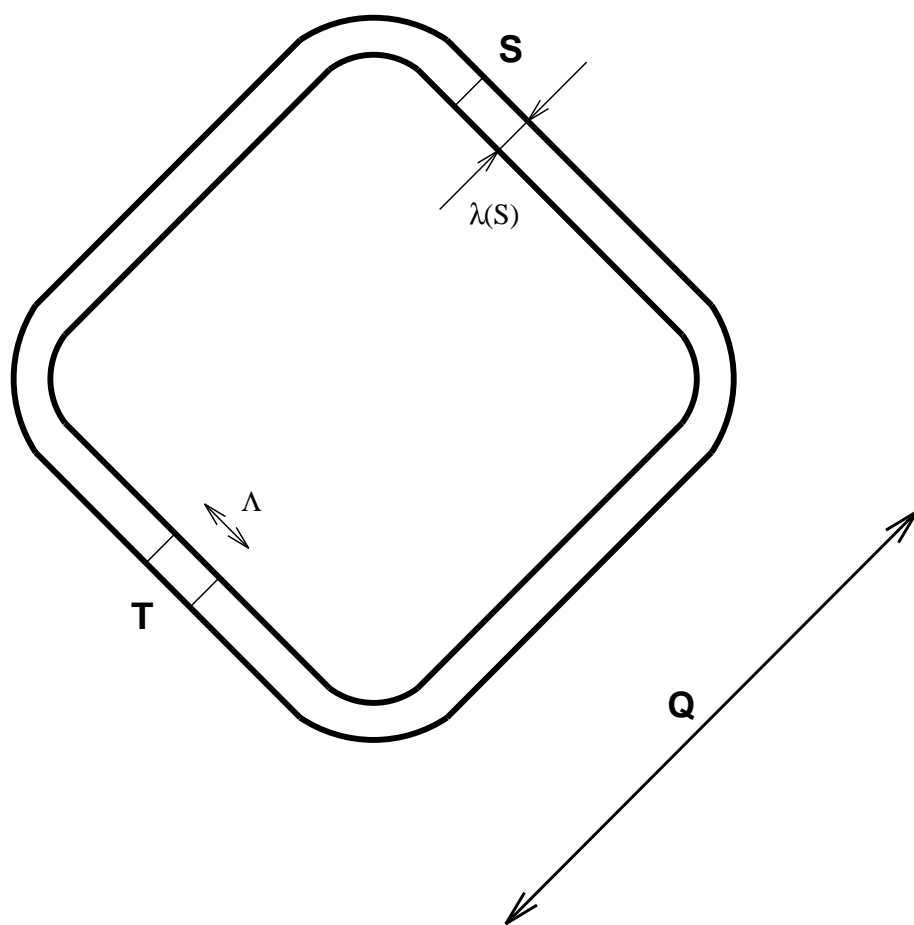


FIG. 1.

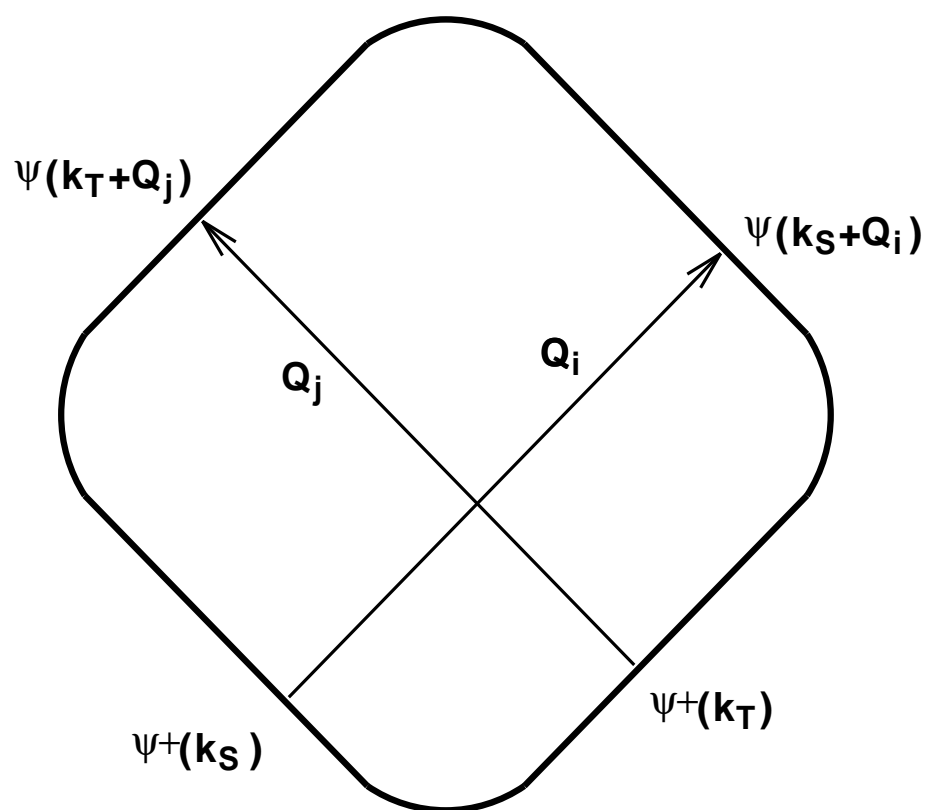


FIG. 2.

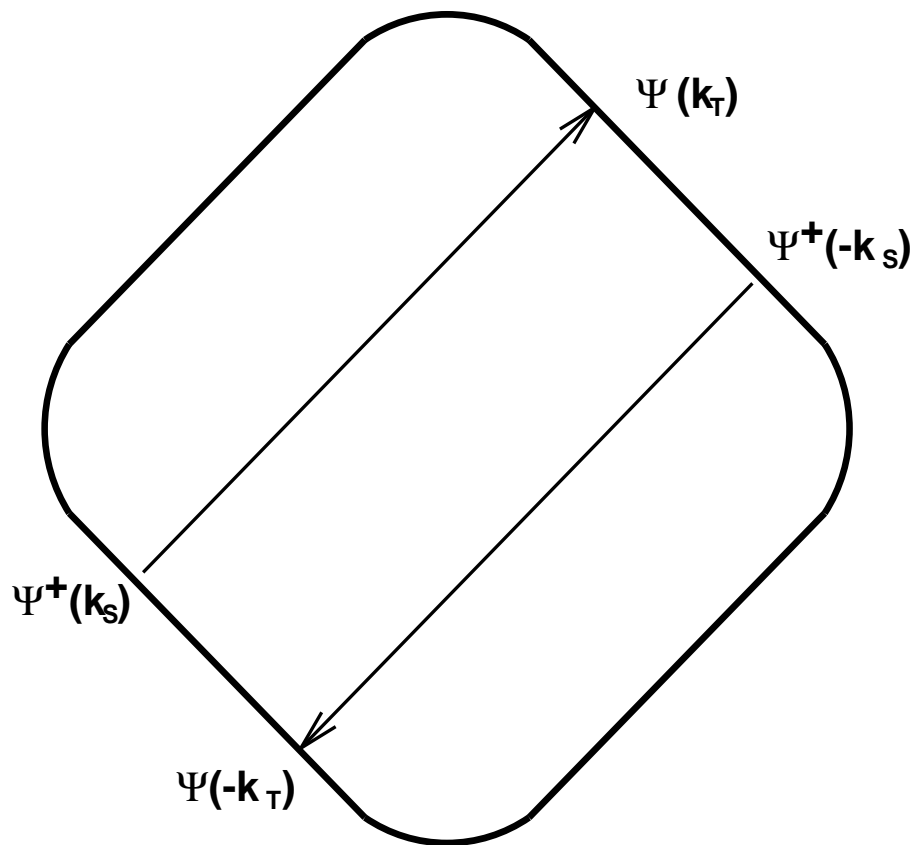


FIG. 3.

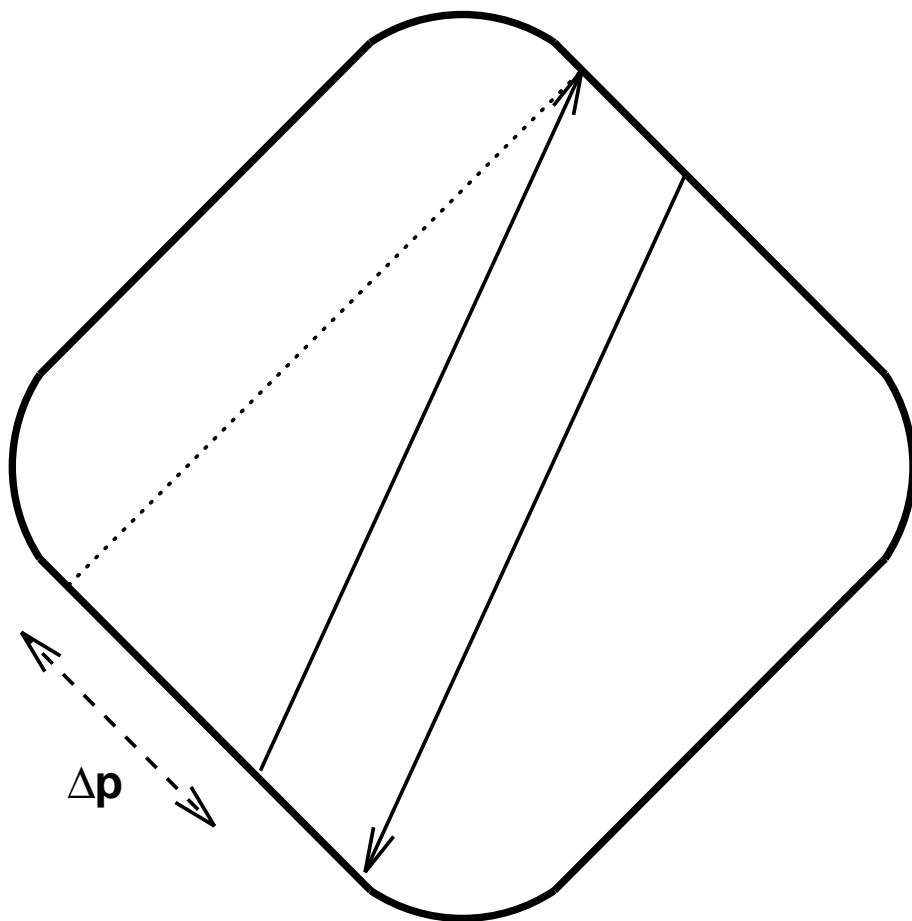


FIG. 4.

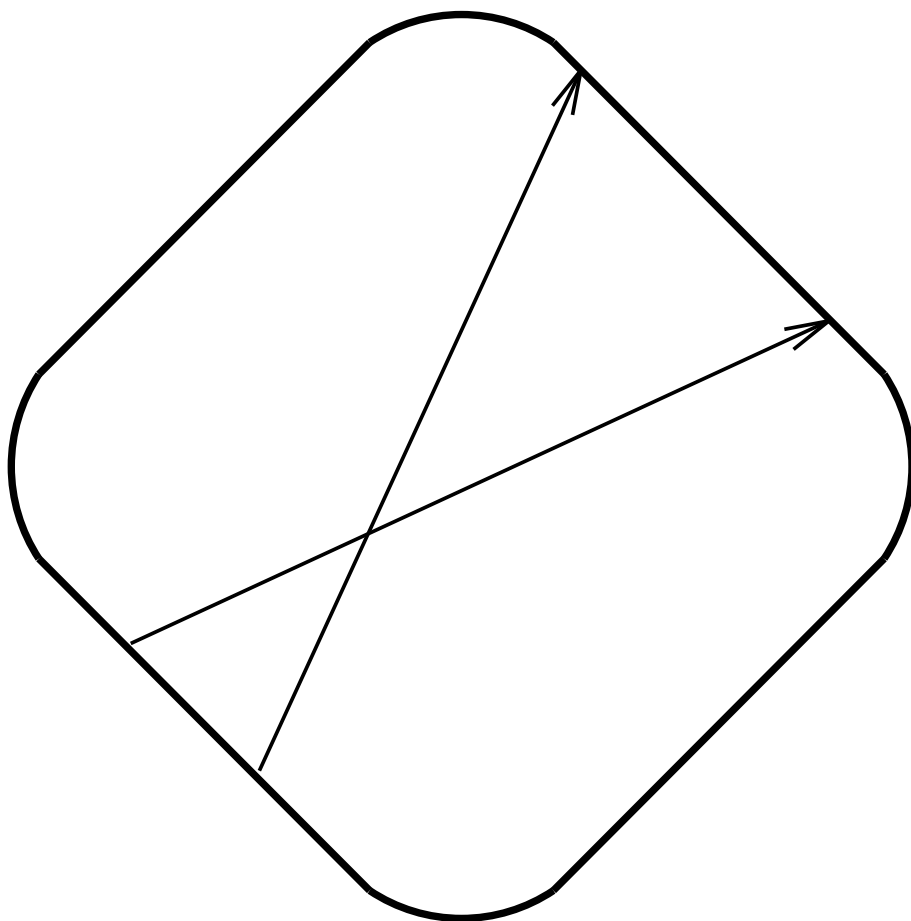


FIG. 5.